Pergamon

0301-9322(93)E0007-R

Int. J. Multiphase Flow Vol. 20, No. 2, pp. 339–353, 1994
Copyright © 1994 Elsevier Science Ltd
Printed in Great Britain. All rights reserved
0301-9322/94 $7.00 + 0.00

THE INERTIAL LIFT ON A RIGID SPHERE TRANSLATING IN A LINEAR SHEAR FLOW FIELD

P. CHERUKAT,[1] J. B. MCLAUGHLIN[1]† and A. L. GRAHAM[2]

[1]Department of Chemical Engineering, Clarkson University, Potsdam, NY 13699-5705, U.S.A.

[2]Los Alamos National Laboratory, Los Alamos, NM 87545, U.S.A.

(Received 20 February 1993; in revised form 10 October 1993)

Abstract—The shear-induced inertial migration of a rigid sphere has been studied experimentally using a homogeneous shear flow apparatus. The experimentally measured migration velocities have been compared with those predicted by the asymptotic formulas previously given by Saffman and McLaughlin. The analysis of a sphere translating in a shear field in the presence of a single wall has been extended to the case of a sphere translating in a fluid undergoing a uniform shear between two parallel walls.

Key Words: inertia, lift, shear, wall

1. INTRODUCTION

It has been observed experimentally that rigid spherical particles in a laminar shear field tend to migrate laterally (i.e. they experience a lift force if they are constrained from moving laterally). This phenomenon has been observed even when the Reynolds number based on a characteristic dimension of the particle and a characteristic velocity of the flow is small but finite. Creeping-flow equations are time reversible and do not predict any lateral migration or lift on particles in a shear field. Hence, it can be concluded that inertial effects cause the particles to migrate laterally.

The inertial lift on a sphere translating in a linear unbounded shear flow field was analyzed by Saffman (1965). Using matched asymptotic expansions, Saffman derived an expression that gives the lift force on the sphere to the lowest order. This expression is valid when all the Reynolds numbers (defined in section 2) are small compared to unity and for slow translation of the sphere. McLaughlin (1991) derived an expression for the migration velocity of a sphere in a shear flow for arbitrary ratios of the Reynolds number based on the translation (relative) velocity and the diameter of the sphere and the square root of the Reynolds number based on the shear and the diameter of the sphere. He also assumed that both these Reynolds numbers are small in magnitude compared to unity. McLaughlin's (1991) expression reduces to Saffman's (1965) expression when the relative magnitudes of the two Reynolds numbers approach the appropriate limit (this is described in section 2). A related problem is that of a sphere rotating and translating in a quiescent fluid. Rubinow & Keller (1961) analyzed this problem and obtained an expression for the lift force on the sphere. A rigid sphere in a linear shear flow will rotate and this rotation can cause an additional lift force. Auton (1987) considered the lift force on a sphere in a weak shear flow when the change in the incident velocity of the undisturbed flow field across the sphere is small compared to the relative velocity of the sphere. The lift force was calculated by assuming that the flow is inviscid.

The lift force on a sphere in wall-bounded flows when the wall lies in the inner region of the sphere's disturbance flow has been analyzed by many authors. These analyses are applicable if the distance between the wall and the sphere is very small compared to the length scales at which the inertial effects become important. Cox & Brenner (1968) considered the general problem of a nonneutrally buoyant sphere sedimenting near a flat wall in a linear shear flow field. They assumed that the distance between the particle and the wall is large compared to the radius of the particle and the inertial migration velocity was obtained in terms of integrals involving the Green's

†To whom all correspondence should be addressed.

functions for the creeping-flow equations. Ho & Leal (1974) considered the lift on a neutrally buoyant sphere in a planar flow bounded by two flat walls. These authors assumed that the walls lie in the inner region of the sphere's disturbance flow and derived an expression for the lift force. This expression is valid when the sphere is not very close to the walls. Cox & Hsu (1977) evaluated the Green's functions in Cox & Brenner's (1968) analysis and derived an analytical expression for the lift force on a rigid sphere sedimenting near a wall in a quadratically varying flow. This analysis can be simplified to give the lift force on a sphere translating in a linear shear flow field near a flat wall. Vasseur & Cox (1976) extended this analysis to the case of a sphere translating in quadratically varying and linear shear flows bounded by two flat walls. Leighton & Acrivos (1985) derived an expression for the lift force on a stationary rigid sphere which is in contact with a flat wall in a linear shear flow field. The lift on a rigid sphere in a linear shear flow, when the distance between the wall and the sphere is comparable to the radius of the sphere, has been analyzed by Cherukat & McLaughlin (1994). Lovalenti considered the lift on a sphere in a linear shear flow near a wall when the wall lies in the inner region (see Cherukat & McLaughlin 1994). Using far-field approximations for the disturbance flow due to the sphere, an expression for the lift force which is valid when the sphere is far from the wall was derived.

Drew (1988) considered the problem of a sphere in a strong shear field (corresponding to Saffman's limit) near a flat wall. A fourth-order ordinary differential equation was solved numerically to obtain the Fourier transform of the velocity field and the migration velocity was evaluated by numerical quadrature. McLaughlin (1993) analyzed the problem of a sphere sedimenting in a shear field near a flat wall when the wall lies in either the inner or the outer region and an analytical expression for the Fourier transform of the migration velocity was obtained and the migration velocity was computed by evaluating the Fourier integrals numerically. This analysis is valid when the distance between the wall and the sphere is large compared to the radius of the sphere.

The experimental studies of the shear-induced inertial lift reported to date pertain to circular tube flows or two-dimensional Poiseuille flows (Oliver 1962; Repetti & Leonard 1964; Jeffrey & Pearson 1965). In this paper, experiments for spheres translating in linear shear fields will be described and the experimental results will be compared with the predictions of various asymptotic theories. We were primarily interested in the inertial lift on particles which translate with a nonzero relative velocity in a shear field. The experiments were conducted with negatively buoyant spheres. To obtain an estimate of the wall effects on our experimental measurements, we have extended McLaughlin's (1993) results to the case of a sphere translating in a shear flow between two flat parallel walls. The results indicate that the wall effects were small for the measurements that we will present.

This study was motivated by the fact that the inertial lift could affect the motion of aerosol particles in a turbulent channel flow. In a wall-bounded turbulent flow of a gas containing aerosol particles, when the particles move in the viscous sublayer near the walls, the particles can develop Reynolds numbers which are of ordinary unity (McLaughlin 1989), and the presence of the solid boundary and a large velocity gradient can give rise to a lift force that can affect the trajectory of the aerosol particles.

2. SPHERE TRANSLATING IN AN UNBOUNDED SHEAR FIELD

Consider a rigid sphere of radius a in an unbounded shear flow of a fluid of density ρ and kinematic viscosity ν. The sphere is assumed to be located at the origin of a Cartesian coordinate system (figure 1). The undisturbed velocity field is given by $Gx\mathbf{e}_3$, where G is the velocity gradient in the x direction and $\mathbf{e}_1$, $\mathbf{e}_2$ and $\mathbf{e}_3$ are unit vectors in the x, y and z directions. The sphere translates with a velocity $-V_s\mathbf{e}_3$ and rotates with an angular velocity $\boldsymbol{\Omega}$. Reynolds numbers based on the shear, relative (sedimentation) velocity and angular velocity are defined by

$$\mathrm{Re}_G = \frac{4a^2G}{\nu}, \quad \mathrm{Re}_S = \frac{2aV_s}{\nu} \quad \text{and} \quad \mathrm{Re}_\Omega = \frac{4a^2\Omega}{\nu}, \qquad [1]$$

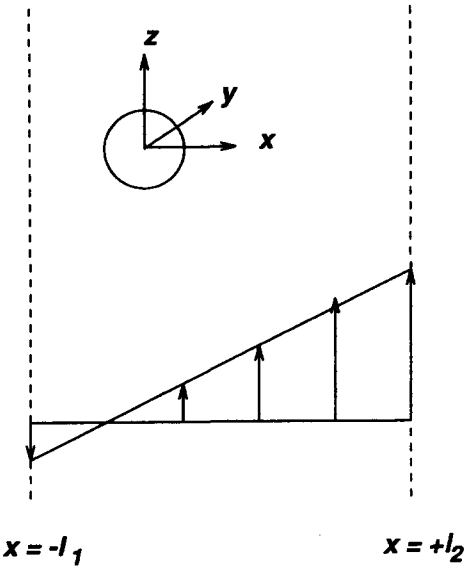

Figure 1. Coordinate system for a sphere sedimenting in a linear shear flow field.

respectively. The quantity $\mathrm{Re_S}$ will be referred to as the slip Reynolds number. It is assumed that

$$\mathrm{Re_S} \ll 1,\ \mathrm{Re_G} \ll 1 \text{ and } \mathrm{Re_\Omega} \ll 1. \quad [2]$$

In the region in which the inertial terms are comparable to the viscous terms (the outer region), to leading order, the Navier–Stokes equations can be linearized and expressed as (see McLaughlin 1991):

$$(V_s + Gx)\frac{\partial \mathbf{v}}{\partial z} + Gv_1\mathbf{e}_3 = -\nabla P + \nu\nabla^2\mathbf{v} - 6\pi a\nu V_s\mathbf{e}_3\delta(\mathbf{r}), \quad [3]$$

where $\mathbf{v}$ is the disturbance velocity, v_1 is the x component of the disturbance velocity, P is the pressure divided by the density and δ is the three-dimensional delta function. The Stokes length, L_S, is defined as

$$L_S = \frac{\nu}{V_s}; \quad [4]$$

and the Saffman length, L_G, is defined as

$$L_G = \left(\frac{\nu}{G}\right)^{1/2}. \quad [5]$$

The inertial terms are comparable to the viscous terms at distances which are $O(\min(L_G, L_S))$ (see Proudman & Pearson 1957; Saffman 1965). Saffman (1965) assumed that

$$L_G \ll L_s \quad [6]$$

or, equivalently,

$$\mathrm{Re_G^{1/2}} \gg \mathrm{Re_S}, \quad [7]$$

and obtained an expression for the migration velocity of the sphere. Saffman's expression for the migration velocity V_m^u is

$$V_m^u = 0.343 a V_s\left(\frac{G}{\nu}\right)^{1/2} \quad [8]$$

(In subsequent discussions, the superscript u will denote an unbounded flow field.) McLaughlin (1991) generalized Saffman's analysis by removing restriction [7] and obtained an expression for the migration velocity. The only assumption is that the Reynolds numbers defined in [1] are small

compared to unity. McLaughlin's expression for the migration velocity in an unbounded linear shear flow field is

$$V_m^u = \frac{3}{2\pi^2} a V_s \left(\frac{G}{\nu}\right)^{1/2} J^u(\varepsilon), \quad [9]$$

where ε is defined by

$$\varepsilon = \frac{\mathrm{Re}_G^{1/2}}{\mathrm{Re}_S} \quad [10]$$

and J^u is a three-dimensional integral that is a function of ε. When ε is large, [9] reduces to Saffman's expression for the migration velocity. When ε is small, [9] predicts a very small migration velocity and for $\varepsilon < 0.2$ the integral J^u has very small negative values. The integral J^u can be considered to be a nondimensional lift force which has the value 2.255 when $\varepsilon \to \infty$ (the Saffman limit).

3. WALL EFFECTS

The lateral migration of a sphere sedimenting in a linear shear flow field near a planar rigid wall when the distance from the wall is very large compared to the radius of the sphere has been analyzed by McLaughlin (1993). An analytical expression for the Fourier transform of the migration velocity was obtained by superposition. In this section we will extend this method to the case where the sphere translates in a linear shear flow bounded by two planar walls. The two planar walls are located at $x = -l_1$ and $x = +l_2$ and it is assumed that $l_1, l_2 \gg a$.

The two-dimensional Fourier transform of the velocity field, $\boldsymbol{\Gamma}$, is defined as

$$\boldsymbol{\Gamma} = (\Gamma_1, \Gamma_2, \Gamma_3)^T = \frac{1}{4\pi^2} \int_{-\infty}^{\infty} \int_{-\infty}^{\infty} \mathbf{v} \exp[-i(k_2 y + k_3 z)] \, dy \, dz, \quad [11]$$

where i is $\sqrt{-1}$. Equation [3] can be transformed into the Fourier space using [11]. Using the continuity equation, pressure can be eliminated and a fourth-order differential equation can be obtained for Γ_1^u. This differential equation can be expressed in nondimensional form as

$$\left[iq_3\left(\frac{1}{\varepsilon} + x_*\right) - \left(\frac{\partial^2}{\partial x_*^2} - p^2\right)\right]\left[\frac{\partial^2}{\partial x_*^2} - p^2\right]\Gamma_1^{*u} = \frac{3iq_3}{\pi \, \mathrm{Re}_G^{1/2}} \frac{d\delta(x_*)}{dx_*}. \quad [12]$$

The dimensionless quantities x_*, $\mathbf{q}$, $\boldsymbol{\Gamma}^*$ and p are defined by

$$x_* = \frac{x}{L_G}, \quad \mathbf{q} = L_G k, \quad \boldsymbol{\Gamma}^* = \frac{\boldsymbol{\Gamma}}{a^2 V_s} \text{ and } p = \sqrt{q_2^2 + q_3^2}. \quad [13]$$

The operator on the left-hand side of [12] can be factorized and [12] can be expressed as

$$L_1 L_2 \Gamma_1^{*u} = \frac{3iq_3}{\pi \, \mathrm{Re}_G^{1/2}} \frac{d\delta(x_*)}{dx_*}, \quad [14]$$

where

$$L_1 = \frac{\partial^2}{\partial\left[\gamma x_* + \dfrac{\beta^2}{\gamma^2}\right]^2} - \left[\gamma x_* + \frac{\beta^2}{\gamma^2}\right] \quad [15]$$

and

$$L_2 = \frac{\partial^2}{\partial x_*^2} - p^2. \quad [16]$$

The quantities γ and β are defined by

$$\gamma = (iq_3)^{1/3}, \quad |\arg(\gamma)| = \frac{\pi}{6} \quad [17]$$

and

$$\beta^2 = p^2 + \frac{iq_3}{\varepsilon}. \quad [18]$$

The solution of [14] is

$$\Gamma_1^{*u} = \frac{\exp(px_*)}{2p}\int_{\infty}^{x_*}\exp(-ps)f(s)\,ds - \frac{\exp(-px_*)}{2p}\int_{-\infty}^{x_*}\exp(ps)f(s)\,ds, \quad [19]$$

where f is defined as

$$f(x_*) = \frac{-3iq_3\,\mathrm{Ai}\left(\gamma x_* + \frac{\beta^2}{\gamma^2}\right)}{\gamma\pi\,\mathrm{Re}_G^{1/2}\,\mathrm{Ai}(0)\mathrm{Ai}'(0)(\omega^2-1)}\left[\frac{\partial}{\partial s}\,\mathrm{Ai}\left(\omega^2\left(\gamma s + \frac{\beta^2}{\gamma^2}\right)\right)\right]_{s=0}, \quad [20]$$

for $x > 0$, and

$$f(x_*) = \frac{-3iq_3\,\mathrm{Ai}\left(\omega^2\left(\gamma x_* + \frac{\beta^2}{\gamma^2}\right)\right)}{\gamma\pi\,\mathrm{Re}_G^{1/2}\,\mathrm{Ai}(0)\mathrm{Ai}'(0)(\omega^2-1)}\left[\frac{\partial}{\partial s}\,\mathrm{Ai}\left(\gamma s + \frac{\beta^2}{\gamma^2}\right)\right]_{s=0}, \quad [21]$$

for $x < 0$. The function Ai is the Airy function and ω is defined to be $\exp(-2\pi i/3)$ when $q_3 > 0$ and $\exp(2\pi i/3)$ when $q_3 < 0$. In general, the integrals in [18] have to be evaluated numerically. The details of these computations can be found in McLaughlin (1993). For values of $|x_*|$ that are large compared to unity, the Fourier transform of the disturbance flow is

$$\Gamma_1^{*u} = \frac{0.2241q_3^{2/3}}{\mathrm{Re}_G^{1/2}\,p}\exp(-p\,|x_*|). \quad [22]$$

The derivation of this expression may also be found in McLaughlin (1993). The effect of the walls at $x_* = -l_1^*$ and $x_* = +l_2^*$ on the migration velocity can be obtained by superposition of the wall disturbance on the disturbance flow in an unbounded fluid at the location of the particle. If $\boldsymbol{\Gamma}^{*w}$ denotes the Fourier transform of the disturbance flow due to the walls, then the Fourier transform of the total disturbance flow, $\boldsymbol{\Gamma}^*$, is given by

$$\boldsymbol{\Gamma}^* = \boldsymbol{\Gamma}^{*w} + \boldsymbol{\Gamma}^{*u}. \quad [23]$$

The wall disturbance satisfies the homogeneous differential equation

$$L_1 L_2 \Gamma_1^{*w} = 0. \quad [24]$$

The solution of $L_1 f^w = 0$ is given by

$$f^w = \mathrm{C}_1\,\mathrm{Ai}\left(\gamma x_* + \frac{\beta^2}{\gamma^2}\right) + \mathrm{C}_2\,\mathrm{Ai}\left(\omega^2\left(\gamma x_* + \frac{\beta^2}{\gamma^2}\right)\right). \quad [25]$$

Using [17], it can be shown that the function $\mathrm{Ai}(\gamma s + \beta^2/\gamma^2)$ decays rapidly for large positive values of s and that the function $\mathrm{Ai}(\omega^2(\gamma s + \beta^2/\gamma^2))$ decays rapidly for large negative values of s.

The solution of the linear differential equation

$$L_2\Gamma_1^{*w} = f^w \quad [26]$$

can be obtained by the method of variation of parameters and is given by

$$\Gamma_1^{*w} = \frac{\exp(px_*)}{2p}\int_{l_2^*}^{x_*}\exp(-ps)f^w(s)\,ds - \frac{\exp(-px_*)}{2p}\int_{-l_1^*}^{x_*}\exp(ps)f^w(s)\,ds + \mathrm{D}_1\exp(-px_*) + \mathrm{D}_2\exp(px_*). \quad [27]$$

The boundary conditions for Γ_1^{*w} are

$$\Gamma_1^{*w} = -\Gamma_1^{*u} \quad \text{at } x_* = -l_1^* \text{ and } x_* = +l_2^*, \quad [28]$$

and

$$\frac{d\Gamma_1^{*w}}{dx_*} = -\frac{d\Gamma_1^{*u}}{dx_*} \quad \text{at } x_* = -l_1^* \text{ and } x_* = +l_2^*. \quad [29]$$

Using [28] and [29], the constants D_1, D_2, C_1 and C_2 can be determined. These constants are given by

$$D_1 = \frac{\exp(-pl_1^*)}{2}\left[-\Gamma_1^{*u}(-l_1^*) + \frac{1}{p}\frac{d\Gamma_1^{*u}}{dx_*}\bigg|_{-l_1^*}\right], \quad [30]$$

$$D_2 = \frac{\exp(-pl_2^*)}{2}\left[\Gamma_1^{*u}(l_2^*) + \frac{1}{p}\frac{d\Gamma_1^{*u}}{dx_*}\bigg|_{l_2^*}\right], \quad [31]$$

$$C_1 = 2p\exp[p(l_1^* + l_2^*)]\frac{[R_1\exp(-pl_2^*)F_B + R_2\exp(-pl_1^*)E_B]}{[E_BF_A - E_AF_B]} \quad [32]$$

and

$$C_2 = -2p\exp[p(l_1^* + l_2^*)]\frac{[R_1\exp(-pl_2^*)F_A + R_2\exp(-pl_1^*)E_A]}{[E_BF_A - E_AF_B]}, \quad [33]$$

where

$$R_1 = \Gamma_1^{*u}(-l_1^*) + D_1\exp(pl_1^*) + D_2\exp(-pl_2^*), \quad [34]$$

$$R_2 = \Gamma_1^{*u}(l_2^*) + D_1\exp(-pl_2^*) + D_2\exp(pl_1^*), \quad [35]$$

$$E_A = \int_{-l_2^*}^{l_1^*}\exp(-ps)\mathrm{Ai}\left(\gamma s + \frac{\beta^2}{\gamma^2}\right)ds, \quad [36]$$

$$E_B = \int_{l_2^*}^{-l_1^*}\exp(-ps)\mathrm{Ai}\left(\omega^2\left(\gamma s + \frac{\beta^2}{\gamma^2}\right)\right)ds, \quad [37]$$

$$F_A = \int_{-l_1^*}^{l_2^*}\exp(ps)\mathrm{Ai}\left(\gamma s + \frac{\beta^2}{\gamma^2}\right)ds \quad [38]$$

and

$$F_B = \int_{-l_1^*}^{l_2^*}\exp(ps)\mathrm{Ai}\left(\omega^2\left(\gamma s + \frac{\beta^2}{\gamma^2}\right)\right)ds. \quad [39]$$

When $l_1^*, l_2^* \gg 1$, the dominant contributions to the integrals involving $\mathrm{Ai}(\gamma s + \beta^2/\gamma^2)$ come from the region in which $s < 0$ and the dominant contributions to the integrals involving $\mathrm{Ai}(\omega^2(\gamma s + \beta^2/\gamma^2))$ come from the region in which $s > 0$. It can then be shown that the constants in [27] are

$$D_1 = D_2 = 0, \quad [40]$$

$$C_1 = \frac{2p\exp[p(l_1^* + l_2^*)]}{\displaystyle\int_{-l_1^*}^{0}\mathrm{Ai}\left(\gamma s + \frac{\beta^2}{\gamma^2}\right)ds}\left\{\frac{\Gamma_1^{*u}(-l_1^*) - \exp[-p(l_1^* + l_2^*)]\Gamma_1^{*u}(l_2^*)}{-\exp[-p(l_1^* + l_2^*)] + \exp[p(l_1^* + l_2^*)]}\right\} \quad [41]$$

and

$$C_2 = -\frac{2p\exp[p(l_1^* + l_2^*)]}{\displaystyle\int_{l_2^*}^{0}\mathrm{Ai}\left(\omega^2\left(\left(\gamma s + \frac{\beta^2}{\gamma^2}\right)\right)\right)ds}\left\{\frac{\Gamma_1^{*u}(l_2^*) - \exp[-p(l_1^* + l_2^*)]\Gamma_1^{*u}(-l_1^*)}{-\exp[-p(l_1^* + l_2^*)] + \exp[p(l_1^* + l_2^*)]}\right\}. \quad [42]$$

Using [22], the Fourier transform of the disturbance flow due to the walls when the walls are very far from the sphere can be expressed as

$$\Gamma_1^{*w} = \frac{-0.2241}{\mathrm{Re}_G^{1/2}\{1 - \exp[-2p(l_1^* + l_2^*)]\}}\left(\frac{q_3^{2/3}}{p}\right)(\exp(-2pl_1^*) + \exp(-2pl_2^*) - 2\exp[-2p(l_1^* + l_2^*)]). \quad [43]$$

The denominator in [43] can be expanded using the binomial theorem and Γ_1^{*w} can be expressed as an infinite series of the form

$$\Gamma_1^{*w} = \frac{-0.2241}{Re_G^{1/2}}\left(\frac{q_3^{2/3}}{p}\right)(\exp(-2pl_1^*) + \exp(-2pl_2^*) - 2p\exp[-2p(l_1^* + l_2^*)] + \exp[-2p(2l_1^* + l_2^*)] + \exp[-2p(l_1^* + 2l_2^*)] - 2\exp[-2p(2l_1^* + 2l_2^*)] + \cdots). \quad [44]$$

The change in migration velocity due to the walls can be obtained by evaluating the Fourier integral

$$\int_{-\infty}^{\infty}\int_{-\infty}^{\infty} \Gamma_1^{*w}\exp[i(q_2 y + q_3 z)]\,dq_2\,dq_3$$

at $x = y = z = 0$. If V_m^w is the wall contribution to the migration velocity, then

$$V_m^w = -0.2855aV_s\left(\frac{G}{\nu}\right)^{1/2}\left(\frac{1}{(l_1^*)^{5/3}} + \frac{1}{(l_2^*)^{5/3}} - \frac{2}{(l_1^* + l_2^*)^{5/3}} + \frac{1}{(2l_1^* + l_2^*)^{5/3}} + \frac{1}{(l_1^* + 2l_2^*)^{5/3}} - \frac{2}{(2l_1^* + 2l_2^*)^{5/3}} + \cdots\right). \quad [45]$$

The first two terms can be obtained by considering the flow due to image particles at $x_* = -2l_1^*$ and $x_* = 2l_2^*$, and the subsequent terms can be obtained by considering the flow due to successive images. As pointed out by Vasseur & Cox (1977), a boundary-layer argument may be used to estimate the effect of the walls when they are very far from the sphere. If $l_1, l_2 \gg \min(L_S, L_G)$, the flow may be assumed to be inviscid near the walls except in thin boundary layers near the two walls. These boundary layers are of thickness $O(\nu l_1/V_s)^{1/2}$ and $O(\nu l_2/V_s)^{1/2}$. Thus, if l_1 and l_2 are very large compared to the thickness of these boundary layers, the method of images should give a fairly accurate estimate of the effect of the walls on the migration velocity.

The migration velocity of the sphere in the presence of the walls is given by

$$V_m = V_m^u + V_m^w. \quad [46]$$

The dimensionless lift force, J, for a wall-bounded shear flow can be expressed as

$$J = J^u + J^w, \quad [47]$$

where J^w is the wall contribution to the dimensionless lift force. The dimensionless lift force given by [45] for walls which are equidistant (i.e. $l_1^* = l_2^* = l^*$), but very far from the sphere, has been compared with that given by the exact expression [27] in figure 2 for $\varepsilon = \infty$ and $\varepsilon = 1.0$. For values of $\varepsilon > 1.0$, [45] predicts the lift force to within 22% of the value predicted by [27] when the walls are about 10 Saffman lengths away from the sphere. For values of l_1^* and l_2^* that are not large, [27] has to be used to calculate the migration velocity or the lift force. Since [27] involves the integrals of the Airy functions, to evaluate the Fourier transform, the Airy function integrals have to be evaluated numerically. The migration velocity can then be obtained by evaluating the Fourier integral numerically.

In section 4 of this paper, we will describe the measurement of the shear-induced lateral migration velocity of negatively buoyant spheres sedimenting in a linear shear field. The linear shear field was produced by two vertical flat belts moving in opposite directions. To study the shear-induced migration in an unbounded field, the spheres should sediment in a fluid undergoing shear between belts which are very far from the sphere. However, it is not possible to construct such an apparatus. Equation [27] can be used to estimate the effects of the belts on the lateral migration and the experimental conditions can be chosen such that the effects of the bounding walls are minimized.

4. EXPERIMENTAL MEASUREMENT OF THE MIGRATION VELOCITY

In this section we will describe the experimental measurement of lateral migration velocities. A homogeneous shear flow apparatus (HFA) similar to the one used by Graham & Bird (1984) was

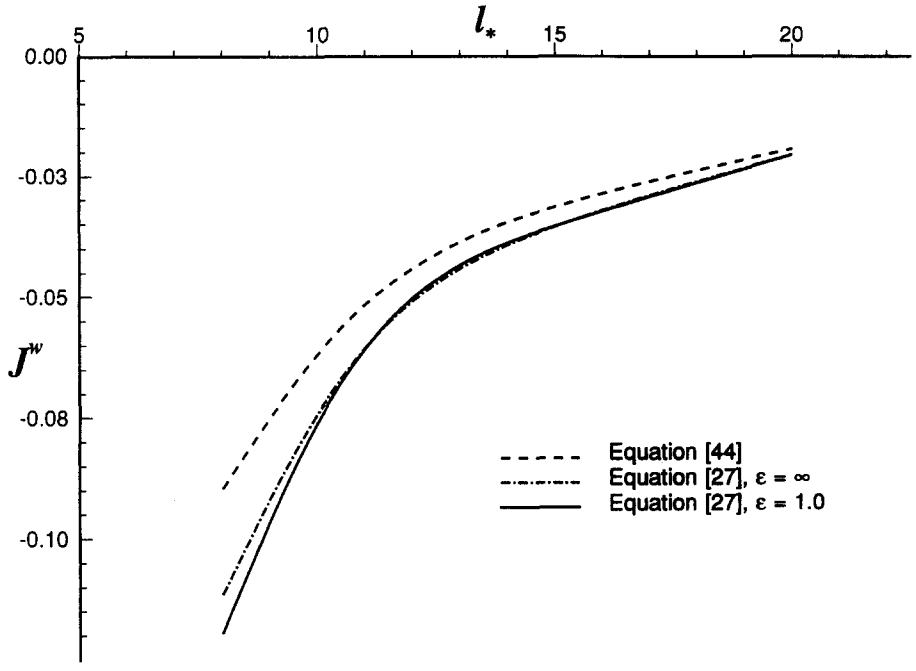

Figure 2. Comparison of J^w predicted by [44] with that predicted by [27] for $\varepsilon = \infty$ and $\varepsilon = 1.0$.

used to create a linear shear flow field. The schematic of the HFA is shown in figure 3. Two rubber timing belts pass over pulleys with matching pitches that rotate in the same sense. Hence the belts move in opposite directions in the viewing section of the HFA. The fluid is contained in the space between the two Plexiglas sheets and the aluminum block. Circular arches (two at each end) are machined in the aluminum block at the top and bottom of the HFA. These semicircular sections ensure that the fluid is subjected to a constant shear (neglecting the small variations in the shear rate in the circular section). The circular arches also reduce the end effects (Graham 1980) by facilitating smooth separation and reentry of the flows at the top and bottom. The belt tensions can be adjusted by a mechanical arrangement. It is necessary to adjust the belt tensions carefully since improperly tensioned belts cause flapping of the belts and walking of the belts along the axis of the pulleys.

To prevent the belts from bowing in the middle of the viewing section, aluminum guide plates (G1 and G2) are fixed. These guide plates also reduce the flapping of the belts and perform better than idler pulleys. Grooves are machined on the Plexiglas sheets to ensure that the belts remain straight while in motion. Sprockets are fixed to the shafts attached to the bottom pulleys P3 and P4 and these are driven by a chain drive attached to a d.c. motor. The speed of the motor can be controlled electronically. At low motor speeds, fluctuations in the belt speeds were noticed. To overcome this problem the gear ratio was changed by using different sprockets. Thus, the motor could be operated at a fairly high speed but the gear reduction ratio ensured that the belts moved at a very low speed. The gap between the belts is 50.8 mm, and the width of each belt is 101.6 mm. For low belt speeds, the speeds were determined by measuring the time required for a mark on the belts to traverse a fixed distance and, at higher speeds, the belt speeds were determined by using a strobe-light focused on the belt teeth. The belt speed was monitored several times during an experiment.

The characteristics of the flow in the HFA depend on the device Reynolds number. A device Reynolds number can be defined as

$$\mathrm{Re}_B = \frac{V_b b}{2\nu}, \qquad [48]$$

where V_b is the belt speed and b is the gap between the belts. To determine the linearity of the flow profile for the experimental conditions, a two-dimensional simulation of the HFA was

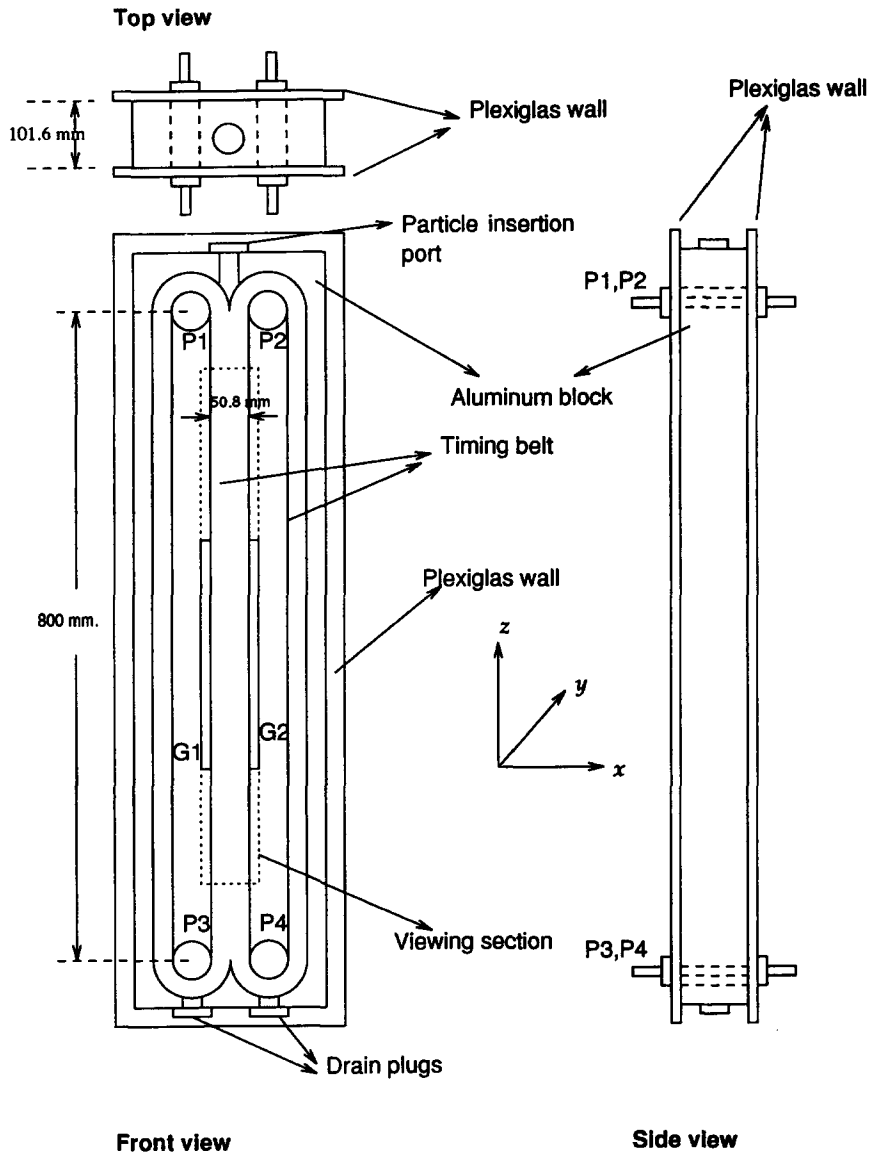

Figure 3. The HFA (homogeneous shear flow apparatus).

performed using the spectral element program NEKTON†. This program could simulate the flow in the exact geometry of the flow path. It was found that the flow remained linear in the test section up to a belt Reynolds number of 60. The flow in the HFA is a three-dimensional flow. A purely two-dimensional shear field can be produced only by belts which are infinitely wide. Very wide belts could not be used since this would have resulted in a very large volume of fluid for the experiments. Also, the belts had to be chosen from commercially available grades. To determine the effect of the aspect ratio (ratio of the gap between the belts to the belt width) on the flow profile, the three-dimensional flow inside the HFA was simulated. Figure 4 shows the iso-velocity contours in the z plane. The simulations show that a two-dimensional flow exists in the middle two-thirds of the HFA. The Plexiglas walls cause the velocity profile to become nonlinear near the walls. To ascertain the linearity of the flow profile experimentally, the velocities of neutrally buoyant polystyrene beads (1 mm dia) were measured by recording their trajectories. The velocity profile obtained by tracking tracer particles for a device Reynolds number of 20 is shown in figure 5.

†NEKTON is a registered trade name of Nektonics Inc. and MIT, Cambridge, MA.

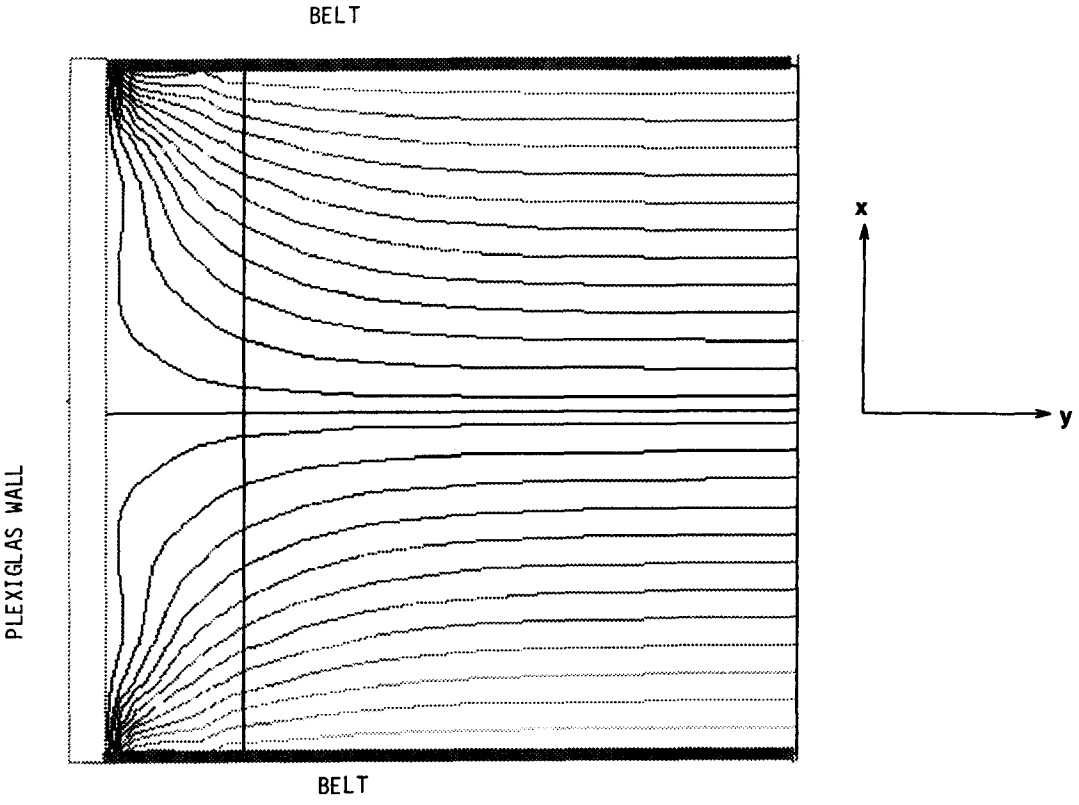

Figure 4. Iso-velocity contours for flow in the HFA when $Re_B = 50.0$, obtained by simulating the flow using the spectral element program NEKTON. Only half of the region between the Plexiglas walls has been shown. The contours in the other half are symmetric. (The solid vertical line near the Plexiglas wall is an imaginary line and corresponds to an element boundary which is generated by the simulation program.)

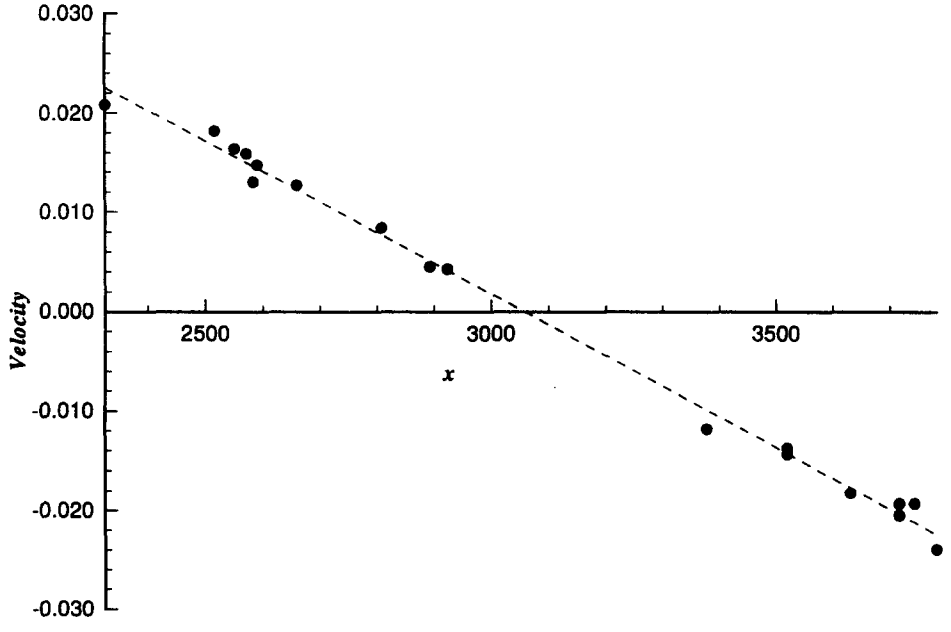

Figure 5. The velocity profile obtained by tracking tracer particles. The values plotted on the x axis correspond to the distance measured on the video monitor using the x–y indicator and the numbers on the x axis are the values of the analog signal generated by the x–y indicator. As the cross hair moves from one end of the screen to the other, the analog signal varies linearly. The velocities plotted on the y axis were obtained by dividing the distance (expressed in terms of the change in the analog signal) by time.

In this study, we were interested in the shear-induced inertial lift on spheres which have a nonzero relative velocity. It was easier to perform experiments with negatively buoyant spheres than with positively buoyant spheres. Plastic spheres (1 mm dia polystyrene spheres, 1.5 mm dia polyacetate spheres and 2 mm dia polyacetate spheres) were used for these experiments. The liquids used in these experiments were mixtures of UCON 50-HB-5100 oil and water. UCON oil is a water-soluble mixture of polyalkene glycols and behaves like a Newtonian fluid. The viscosities and the densities of these mixtures were controlled by adjusting their compositions. For these experiments, the viscosities of the mixtures used were in the range 10–50 cP. It was not necessary to cool the HFA to remove the heat generated by viscous dissipation while using these liquids. The vertical alignment of the HFA was checked optically. The HFA was filled with the UCON oil–water mixture and the solution was allowed to stand for several hours to permit air bubbles to rise to the top and escape through the air vents on the top. The belts were set in motion and, after the flow field had attained a steady state, a plastic sphere was released into the fluid through the particle injection port at the top of the HFA. The sphere sedimented in the plane midway between the two Plexiglas walls. When the sphere reached the test section, its images at two different instants were recorded. The lateral migration velocity was determined from these images.

The image-recording and analyzing system was similar to the one used by Cherukat & McLaughlin (1990) (see figure 6). It consists of two videocameras (Panasonic WV5000) with magnifying lenses. The cameras had 525 scan lines and a horizontal resolution of 650 lines at the center. The cameras are focused on the midplane between the Plexiglas plates of the HFA. The field of view of camera B is located below that of camera A. The vertical distance between the cameras was adjusted so that in the time required by the sphere to pass from the field of view of camera A to that of camera B, it migrates a reasonable distance in the lateral direction. The video synchronizer combines the video signal from both the cameras and displays it as a composite split-screen image. The image of sedimenting spheres were recorded and these images were analyzed using an X–Y indicator (Colorado Video 610E). The X–Y indicator superimposes vertical and horizontal cross hairs on the image. The position of these cross hairs on the video monitor can be determined by measuring the analog signal from the X–Y indicator. The value of the analog signal depends on the position of the cross hairs on the screen. As the cross hairs are moved from one end on the screen to the other, the signal varies linearly. The analog signal was measured using

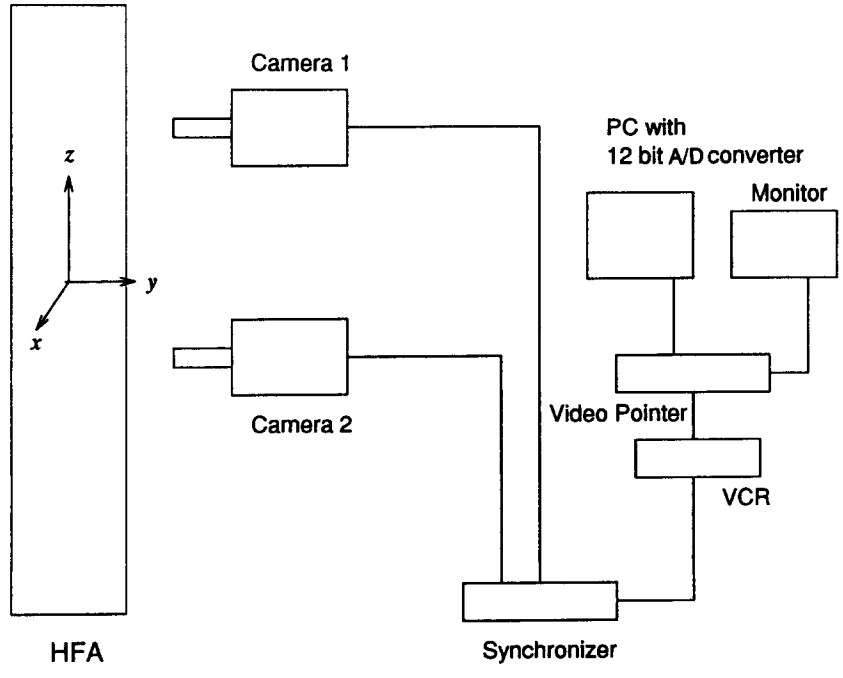

Figure 6. Image-recording and analyzing system used for measuring the shear-induced lateral migration velocities.

a 12-bit A/D board interfaced with a PC. The lateral distance migrated by the sphere was determined by measuring the analog signals when the cross hair is aligned with one of the edges of the image of the sphere when it is in the field of view of camera A and when it is in the field of view of camera B. The difference in the value of the signal was used to determine the distance migrated by the sphere.

The experiments were conducted for a range of slip Reynolds numbers, $Re_S = 0.1$ to 2.5. The experiments for measuring the migration velocities required the measurement of small displacements (typically between 2–4 mm). The elapsed time was measured by counting the number of video frames. The cameras had a frame frequency of 30 frames/s. Thus, the time could be measured to an accuracy of 1/30th s. The factor that could have contributed to the largest experimental error is the inaccuracy in the measurement of distances. One of the possible causes for this is the small misalignment of the HFA. As mentioned before, the alignment of the HFA was checked optically. The cameras were vertically aligned by focusing on a plumb-line and the cameras were then used to align the HFA. The plumb-line used in these experiments was 0.1 mm dia, which when displayed on the screen was slightly larger than size of the $X-Y$ cross hairs. The $X-Y$ cross hairs are the same size as the scan lines on the video monitor. Thus, the accuracy of alignment is determined by the thickness of the plumb-line. The accuracy of the measurements depends also on the calibration accuracy of the cameras. The accuracy of calibration is also determined by the thickness of the plumb-line used for calibration.

In these experiments, when the spheres reached the viewing section (i.e. they were in the field of view of the cameras), the spheres were more than 6 Saffman lengths from the belts. Equation [27] was used to estimate the possible effect of the belts on the observed migration velocities. It was not possible to measure the distance between the sphere and the belts very accurately. However, it should be noted that the lateral distance traveled by the sphere could be measured very accurately. The wall contribution should only be considered as a maximum possible value. The maximum value of the wall contribution was $<15\%$ of the lift in an unbounded shear. On analyzing the scatter in the experimental data, the maximum wall effect was found to be within the margin of experimental error for most of the values of ε. The dimensionless lift force J was calculated using the measured migration velocities for the slip Reynolds numbers, Re_S (i.e. the Reynolds number based on the relative velocity and the diameter of the sphere), in the range 0.2–1.0. These values of J have been compared with the values of J predicted by McLaughlin's expression [9] in figure 7. The experimental data plotted in figure 7 is also given in table 1. The dimensionless lift force when the wall effects are added is also shown in this figure. The experimental data indicate that the lift force decreases with ε, and it can be concluded that, within the margin of experimental error, [9] can be used to predict the shear-induced migration velocity, and that Saffman's expression [8] overpredicts the lift if [7] is not satisfied. The experimental data plotted in figure 7 indicate that the discrepancy in the measured migration velocities and that predicted by [9] increase for $\varepsilon > 1.0$. The experiments for $\varepsilon > 1$ were conducted with 1 mm dia polystyrene spheres sedimenting in a moderately viscous liquid. The sedimentation velocities were quite small in these experiments. This resulted in small migration velocities. Hence, the effect of any error in measuring small displacements (e.g. a small misalignment of the HFA/cameras from the vertical which would appear as a virtual displacement in the lateral direction when the images are analyzed) would cause a larger percentage deviation in the value of J obtained from the experimental measurements.

Several experiments were conducted in which Re_S values were in the range 1.2–2.8. Equation [9] predicts a very small migration velocity when $\varepsilon < 0.20$. The experimental data is shown in table 2. However, in these experiments, the spheres were observed to migrate significantly even when the values of ε were small. Negative migration velocities (i.e. migration of the spheres in the direction opposite to that predicted by Saffman's expression) were not observed in any of these experiments. Equation [9] is a leading-order asymptotic expression for the migration velocity and is strictly valid when $Re_S \ll 1$. Hence, it may not give the correct value of the migration velocity when the value of Re_S is $O(1)$. Rubinow & Keller's (1961) analysis gives an asymptotic expression for the lift force on a sphere rotating and translating in a quiescent fluid when $Re_S \ll 1$. The value of the migration velocity obtained using Rubinow & Keller's expression for the experimental conditions, by assuming that the sphere rotates with an angular velocity which is equal to one-half the velocity

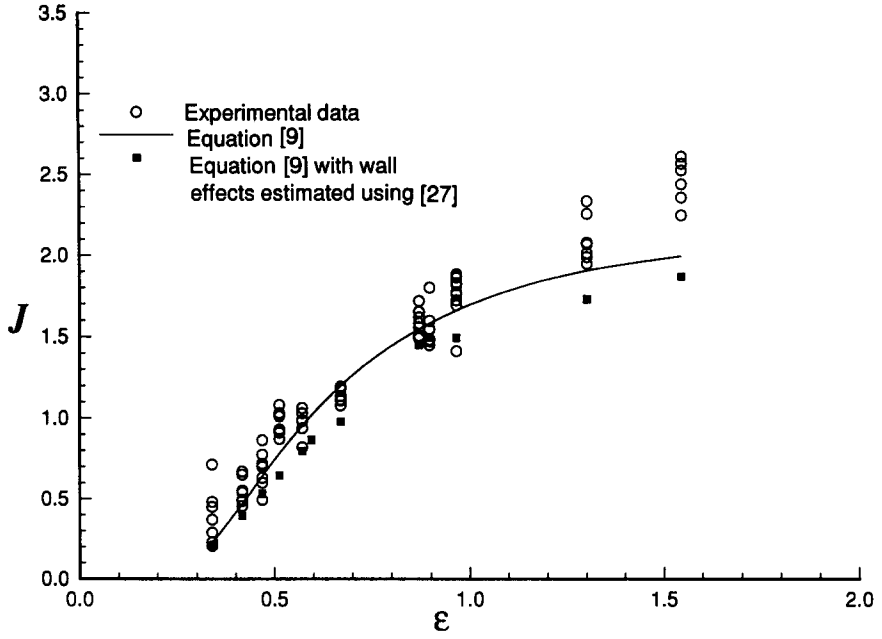

Figure 7. Comparison of J from experimental data with that predicted by McLaughlin's (1991) expression, [9], for $Re_S < 1.0$. The values obtained by adding the wall contribution given by [27] are also shown.

Table 1. Experimentally obtained values of J for $Re_S < 1$ (these data are also plotted in figure 7)

Re_S	Re_G	ε	J, experimental	J, [9]
0.7368	0.0626	0.3395	0.3910	0.2249
0.7542	0.0988	0.4168	0.5494	0.4682
0.6120	0.0822	0.4685	0.6844	0.6391
0.7542	0.1495	0.5126	0.9714	0.7794
0.6662	0.1448	0.5713	0.9682	0.9516
0.4344	0.0668	0.5949	0.9979	1.0154
0.6285	0.1775	0.6703	1.1340	1.1973
0.5608	0.1456	0.6804	1.0736	1.2192
0.3996	0.1211	0.8708	1.5945	1.5440
0.4078	0.1340	0.8977	1.5542	1.5785
0.3156	0.0931	0.9668	1.7597	1.6569
0.2007	0.0683	1.3021	2.0920	1.9021
0.1989	0.0945	1.5455	2.4538	1.9908

Table 2. Migration velocities for $Re_S > 1$

Re_S	Re_G	ε	V_m(mm/s), measured	V_m(mm/s), [8]	V_m(mm/s), Rubinow & Keller (1961)
1.2220	0.0939	0.2512	0.01245	0.00119	0.00273
1.3903	0.2439	0.3552	0.03190	0.01873	0.00936
1.4603	0.2602	0.3493	0.03006	0.01722	0.01016
1.5097	0.3599	0.3973	0.05341	0.03472	0.01413
1.5097	0.4687	0.4535	0.08392	0.05081	0.01840
1.5291	0.1112	0.2181	0.01325	0.00000	0.00446
1.9560	0.2265	0.2432	0.02065	0.00186	0.00985
1.9560	0.3258	0.2918	0.02772	0.00950	0.01472
1.9730	0.2372	0.2468	0.01300	0.00207	0.00951
1.9730	0.1594	0.2023	0.00916	−0.00040	0.00642
2.7809	0.2907	0.1939	0.01285	−0.00081	0.01321
2.7809	0.1906	0.1570	0.00952	−0.00075	0.00866

gradient, is also indicated in table 2. The experimentally measured migration velocities are higher than that predicted by Rubinow & Keller's (1961) expression but the difference between the experimental value and that predicted by Rubinow & Keller's expression decreases as Re_S increases.

5. CONCLUSION

The analysis for a sphere translating parallel to a single wall has been extended to the case in which the sphere translates in a linear shear flow between two walls. This expression reduces to the expression that can be derived by considering the disturbance flow due to successive images when the walls are very far (in terms of Saffman length) from the sphere. The experimental results indicate that McLaughlin's (1991) expression for the inertial lift may be used to predict the inertial lift force when $Re_S < 1.0$. At higher Re_S, significant differences can be noticed. This difference could be due to the fact the asymptotic expression based on the Oseen approximation for the outer flow field is not valid at higher Re_S.

Acknowledgements—This work was supported by the U.S. Department of Energy under Grant DE-FG02-8813919. The numerical computations were done on IBM-RISC workstations in the AVS laboratory at Clarkson University. The authors wish to thank Dr James Abbot and Mr Nick Tetlow of Los Alamos National Laboratory for their help in the fabrication and fine tuning of the HFA.

REFERENCES

AUTON, T. R. 1987 The lift force on a spherical body in a rotational flow. *J. Fluid Mech.* **183,** 199–218.

CHERUKAT, P. & MCLAUGHLIN, J. B. 1990 Wall-induced lift on a rigid sphere. *Int. J. Multiphase Flow* **16,** 899–907.

CHERUKAT, P. & MCLAUGHLIN, J. B. 1994 Inertial lift on a rigid sphere in a linear shear flow field near a flat wall (with an appendix by P. M. Lovalenti). *J. Fluid Mech.* In press.

COX, R. G. & BRENNER, H. 1968 The lateral migration of solid particles in Poiseuille flow: I. Theory *Chem. Engng Sci.* **23,** 147–173.

COX, R. G. & HSU, S. K. 1977 The lateral migration of solid particles in a laminar flow near a plane. *Int. J. Multiphase Flow* **3,** 201–222.

DREW, D. A. 1988 The lift on a small sphere in the presence of a wall. *Chem. Engng Sci.* **43,** 769–773.

GRAHAM, A. L. 1980 Ph.D Thesis, Department of Chemical Engineering, University of Wisconsin—Madison, WI.

GRAHAM, A. L. & BIRD, R. B. 1984 Particle clusters in concentrated suspensions. 1. Experimental observations of particle clusters. *Ind. Engng Chem. Fundam.* **23,** 406–410.

HO, B. P. & LEAL, L. G. 1974 Inertial migration of rigid spheres in two-dimensional uni-directional flows. *J. Fluid Mech.* **65,** 365–400.

JEFFREY, R. C. & PEARSON, J. R. A. 1965 Particle motion in laminar vertical tube flow. *J. Fluid Mech.* **22,** 721–735.

LEIGHTON, D. T. & ACRIVOS, A. 1985 The lift on a small sphere touching a plane in the presence of a simple shear flow. *Z. Agnew. Math. Phys.* **36,** 174–178.

MCLAUGHLIN, J. B. 1989 Aerosol particle deposition in numerically simulated channel flow. *Phys. Fluid.* **A1,** 1211–1224.

MCLAUGHLIN, J. B. 1991 Inertial migration of a small sphere in linear shear flows. *J. Fluid Mech.* **224,** 261–274.

MCLAUGHLIN, J. B. 1993 The lift on a small sphere in wall-bounded linear shear flows. *J. Fluid Mech.* **246,** 249–265.

OLIVER, D. R. 1962 Influence of particle rotation on radial migration in the poiseuille flow of suspensions. *Nature* **194,** 1269–1271.

PROUDMAN & PEARSON, J. R. A. 1957 Expansions at small Reynolds numbers for the flow past a sphere and a circular cylinder. *J. Fluid Mech.* **2,** 237–262.

REPETTI, R. V. & LEONARD, E. F. 1964 Sergré–Silberberg annulus formation: a possible explanation. *Nature* **203,** 1364–1348.

RUBINOW, S. I. & KELLER, J. B. 1961 The transverse force on a spinning sphere moving in a viscous fluid. *J. Fluid Mech.* **11,** 447–459.

SAFFMAN, P. G. 1965 The lift on a small sphere in a slow shear flow. *J. Fluid Mech.* **22,** 385–400.

VASSEUR, P. & COX, R. G. 1977 The lateral migration of spherical particles sedimenting in a stagnant bounded fluid. *J. Fluid Mech.* **80,** 561–591.